

Published in final edited form as:

Biomaterials. 2014 September ; 35(27): 7774–7785. doi:10.1016/j.biomaterials.2014.04.039.

Tri-layered elastomeric scaffolds for engineering heart valve leaflets

Nafiseh Masoumi^{a,b,c,e}, Nasim Annabi^{a,d}, Alexander Assmann^{a,d,g}, Benjamin L. Larson^e, Jesper Hjortnaes^{a,h}, Neslihan Alemdar^a, Mahshid Kharaziha^a, Keefe B. Manning^c, John E. Mayer Jr.^{b,*}, and Ali Khademhosseini^{a,d,f}

^aBiomaterials Innovation Research Center, Department of Medicine, Brigham and Women's Hospital, Harvard Medical School, Harvard-MIT Division of Health Sciences and Technology, Massachusetts Institute of Technology, 65 Landsdowne Street, Cambridge, MA 02139, USA

^bDepartment of Cardiac Surgery, Boston Children's Hospital and Harvard Medical School, 300 Longwood Avenue, Boston, MA 02115, USA

^cDepartment of Bioengineering, The Pennsylvania State University, 205 Hallowell Building, State College, PA 16802, USA

^dWyss Institute for Biologically Inspired Engineering, Harvard University, 3 Blackfan Circle, Boston, MA 02115, USA

^eHarvard-MIT Division of Health Sciences and Technology and The David H Koch Institute for Integrative Cancer Research, Massachusetts Institute of Technology, 500 Main Street, Cambridge, MA 02139, USA

^fDepartment of Physics, Faculty of Science, King Abdulaziz University, P.O. Box 80203, Jeddah 21569, Saudi Arabia

^gDepartment of Cardiovascular Surgery and Research Group for Experimental Surgery, Heinrich Heine University, Medical Faculty, Moorenstr. 5, Dusseldorf 40225, Germany

^hDepartment of Cardiothoracic Surgery, University Medical Center Utrecht, Heidelberglaan 100, Utrecht, Netherlands

Abstract

Tissue engineered heart valves (TEHVs) that can grow and remodel have the potential to serve as permanent replacements of the current non-viable prosthetic valves particularly for pediatric patients. A major challenge in designing functional TEHVs is to mimic both structural and anisotropic mechanical characteristics of the native valve leaflets. To establish a more biomimetic model of TEHV, we fabricated tri-layered scaffolds by combining electrospinning and microfabrication techniques. These constructs were fabricated by assembling microfabricated poly(glycerol sebacate) (PGS) and fibrous PGS/poly(-caprolactone) (PCL) electrospun sheets to develop elastic scaffolds with tunable anisotropic mechanical properties similar to the mechanical characteristics of the native heart valves. The engineered scaffolds supported valvular interstitial cells (VICs) and mesenchymal stem cells (MSCs) growth within the 3D structure and promoted the deposition of heart valve extracellular matrix (ECM). MSCs were also organized and aligned along the anisotropic axes of the engineered tri-layered scaffolds. In addition, the fabricated constructs opened and closed properly in an *ex vivo* model of porcine heart valve leaflet tissue

replacement. The engineered tri-layered scaffolds have the potential for successful translation towards TEHV replacements.

Keywords

Microfabricated elastomer; Electrospinning; Biodegradable scaffold; Anisotropic mechanical properties; Heart valve tissue engineering

1. Introduction

Current approaches for heart valve replacements including advanced bioprosthetic and mechanical heart valves are lifesaving in adults suffering from valvular disease. However, there are several limitations associated with currently available heart valve prostheses. Mechanical valves are thrombogenic and require patients to undergo lifelong anticoagulation therapies [1–4]. Bioprosthetic heart valves have limited durability because of their susceptibility to degradation and calcification [3,5]. An important additional drawback for pediatric patient with valvular diseases is the inability of these replacement valves to grow *in vivo* with the patients, which results in multiple re-operations. Autologous tissue engineered heart valves (TEHV) aim to overcome these limitations by creating living, non-cytotoxic, mechanically analogous heart valve replacements that are able to grow and remodel with the patient [6–12].

Heart valves primarily consist of valvular interstitial cells (VICs) that are surrounded by an endothelial monolayer [13]. The extracellular matrix (ECM) of heart valve leaflets is a complex three-dimensional (3D) tissue, consisting of three interconnected layers; the *zona fibrosa*, the *zona spongiosa* and the *zona ventricularis*, with collagen, glycosaminoglycans (GAGs) and elastin representing the predominant ECM component in these three respective layers [13]. This intricate ECM layered architecture dictates the anisotropic mechanical characteristics of valve leaflets [14–17]. More specifically, leaflet mechanical stiffness and elasticity are attributed to the surface fibrous layers; *zona fibrosa* and *zona ventricularis* [18]. Since valve leaflet function is dependent on this structure, ideally, engineered scaffolds should (a) resemble the native tissue microstructure [14,19], (b) match native mechanical properties and retain anisotropy [16,20], (c) have elastic characteristics in deformation similar to native tissue [21,22], and finally (d) possess a controlled degradation rate that preserves structural integrity while providing support for adequate tissue formation [23] but ultimately do not prevent tissue growth.

A typical TEHV approach is to seed natural [24,25] or synthetic scaffolds with cells [7,23,26–29], culture them in static *in vitro* environments or in bioreactors simulating tissue growth with physiological hemodynamics [30–33], and then implant the cell-seeded constructs *in vivo* [7,8,11,30]. Various cell sources such as vascular-derived smooth muscle cells [33], MSCs [34], VICs [23,29,35], and fibroblasts [28] have been utilized to engineer functional TEHV. Previous studies have aimed to create scaffolds, which mimic the structural complexity of native tissue and provide an appropriate environment for cellular growth and *in vitro* ECM generation [7,8,24,26,28,29]. However, some of the drawbacks associated with these engineered scaffolds have prevented them from successful translation

to *in vivo* models. These limitations include non-physiological stiffness (e.g. non-woven scaffolds) [7,32,36], lack of anisotropic characteristics (e.g. homogenous fibrin gels or fibrous scaffolds comprising of random fibers) [10,23,25,26,37], inappropriate micro-architecture (e.g. non-fibrous scaffolds) [27–29], plastic deformation under stress [23,38] and a lack of suturability (e.g. hydrogel based scaffolds and microfabricated scaffolds) [24,39]. Biodegradable elastomers have been synthesized for cardiovascular tissue engineering for their potential to withstand physiological cyclic loads and viscoelastic properties resembling native tissues [22,40–46]. Among these, poly(glycerol sebacate) (PGS) has been employed extensively due to its elasticity, biocompatibility and controlled degradation rate [28,29,47,48]. However, the modulus of PGS varies between 0.18 and 1.5 MPa depending on curing conditions (time and temperature) and scaffold structure [28,48,49], which is considerably lower than the native leaflet stiffness (4–8 MPa) [18,29].

Previously, the fibroblast and VICs seeded microfabricated PGS scaffolds, with diamond-shaped pores, provided adequate anisotropy matching native leaflet properties while supporting tissue formation and ECM deposition [28,29]. However, these constructs lacked a fibrous structure, and the existence of micropores limited their suturability, impeding their application in *in vivo* studies. To resemble the fibrous structure of native tissues, we recently fabricated electrospun fibrous PGS/poly(caprolactone) (PCL) scaffolds with anisotropic and tunable mechanical properties, including aligned fibers that matched the stiffness of native tissues [38,50]. However, the stress–strain curves for electrospun PGS/PCL scaffolds demonstrated large creep deformation. In addition, the small pore size of these scaffolds (pore size <8 μm) prevented cell migration and ECM deposition through their 3D structures, which limited the formation of a 3D tissue construct [38,50].

Here we aimed to fabricate biomimetic tri-layered elastic scaffold with anisotropic properties similar to the structure and mechanics of the native leaflets. A semi-automated layer-by-layer assembly was applied to fabricate this 3D construct with tunable mechanical properties. We hypothesized that combining PGS/PCL microfibers and microfabricated PGS in a tri-layered construct would provide both elasticity and anisotropy to which matched structural and mechanical properties of native leaflets while simultaneously supporting controlled cellular growth and tissue formation with controlled architecture. This approach could have the potential for successful translation towards a TEHV replacement.

2. Materials and methods

2.1. Fabrication and assembly of tri-layered scaffold

2.1.1. Polymer synthesis—PGS pre-polymer was synthesized through polycondensation of glycerol and sebacic acid (1:1 molar ration) by using previously described procedures by Wang et al. [43]. Briefly, sebacic acid and glycerol with 1:1 molar ratio were reacted at 120 °C in high vacuum (~6.5 Pa) for 24 h to synthesize PGS pre-polymer.

2.1.2. PGS micromolding—The fabrication process used to design the PGS scaffolds, consisting of 2:1 aspect ratio diamond shape pores with approximately 75 μm -thick struts, was previously described in detail [29]. The mold was made from an ultra-high temperature machinable glass-mica ceramic sheet (0.5" thick, 2" \times 2", McMaster-Carr, Elmhurst, IL).

The design was cut through the ceramic sheets using a dicing cutter machine (Kulicke & Soffa Industries, Inc., Fort Washington, PA) with a 90 μm wide saw blade. PGS pre-polymer was then melted around the edges of the ceramic mold and allowed to flow into the channels of the fabricated mold. The PGS pre-polymer was then cured in a vacuum oven under high vacuum (<6.5 Pa) at 160 $^{\circ}\text{C}$ for 8 h. A razor blade was used to cut the fabricated ceramic part away from the bottom sheet to release the polymer scaffold with a 300 μm thick from the ceramic sheet. Prior to the electrospinning process, scaffolds were treated with oxygen plasma cleaner to improve adhesion of fibers on the scaffold layers (100 W for 30 s for each sides using Harrick Plasma (Ithaca, NY)) (Fig. 1A).

2.1.3. Electrospinning and layer by layer assembly—A directional electrospinning system was employed to spin the pre-polymers into sheets. The pre-polymer mixture was pushed from a syringe pump at a flow rate of 2 ml/h and 18 kV. The distance from the tip of the gauge needle to the microfabricated scaffolds was set at 18 cm. The microfabricated PGS was placed between two aluminum electrodes (separated by 1.5 cm) and aligned fibers were created between two grounded electrodes for approximately 15 min on either side. The tri-layered scaffolds were then desiccated in a vacuum chamber overnight for solvent evaporation before further characterization (Fig. 1B). The fabricated construct resembled the native leaflets tri-layered structure shown in Fig. 1C.

2.2. Valve leaflet dissection and VICs/MSCs isolation

Leaflets were aseptically excised from fresh sheep hearts, obtained from the Animal Research Facility (ARCH) in Children's Hospital (Boston, MA) under an official review panel approved protocol. Individual leaflets were excised and rinsed thoroughly in a 2% (v/v) solution of antibiotic-antimycotic in Hank's Balanced Salt Solution (HBSS, Invitrogen, Carlsbad, CA) to remove any remaining blood cells. The samples were cut in circumferential and radial directions for further mechanical characterization. The remaining tissues were used for VIC isolation or frozen for biochemical assays.

Bone marrow samples were obtained from sheep femurs in ARCH. Prior to the isolation process the samples were preserved in isolation buffer (ACD solution and heparin sulfate (American Pharmaceutical Partners)) on ice. 15 ml of Ficoll-Paque Plus (Amersham Pharmacia) was added to each 50 ml Accuspin tube (Sigma-Aldrich, A2055) and spun for 1 min (1200 rpm) to sediment the Ficoll-Paque. The mononuclear cell layer was collected with a syringe and transferred into 50 ml conical tubes on ice. Every 10 ml of collected cells were mixed with 5 ml isolation buffer. The cell pellet was obtained following two sequential spinning and resuspension cycles in isolation buffer. The cells were then ready for cultivation and further harvest.

Pulmonary VICs were isolated as described previously by collagenase digestion [29]. Briefly, the leaflets were wiped with sterile gauze to remove the valvular endothelial cells. VICs were then isolated through digestion of the leaflet tissue in a solution of 0.5% (w/v) type I collagenase (Worthington Biochemical) in HBSS at 37 $^{\circ}\text{C}$ for 6 h. The digested tissues were then centrifuged at $1000 \times g$ for 10 min and the isolated cells were then resuspended and expanded in culture medium of Dulbecco's Modified Eagle Medium

(DMEM) supplemented with 10% (v/v) fetal bovine serum and 1% (v/v) antibiotic (pen/strep).

2.2.1. Cell seeding—In preparation for cell seeding, scaffolds were first sterilized by soaking in 70% ethanol for 30 min followed by high intensity UV exposure (800 mW) for 5 min on each side. The scaffolds were then soaked in culture medium for 2 days prior to seeding to improve cell attachment. Each scaffold was then placed into a sterile-vented 50 ml bioreactor tube (TPP Techno Plastic Products AG, Trasadingen, Switzerland). Confluent flasks of sheep pulmonary VICs and MSCs were trypsinized (0.25% (w/v) trypsin, 1 mM EDTA; Invitrogen) and resuspended in culture medium such that 8 ml of cell solution was added to each 50 ml tube resulting in a cell density of approximately 1×10^6 cells/cm². The tubes were then rotated for 24 h inside an incubator at 37 °C and 5% CO₂. After cell attachment, the scaffolds were placed in to individual wells of a non-adhesive 6 well plate (Costar Ultra Low Attachment; Coming, NY) and were subjected to static cell seeding by applying approximately 1×10^6 cells/250 µl media on either side of each scaffold.

2.3. Mechanical testing

Native tissues, single and tri-layered scaffolds were tested by using a uniaxial mechanical Instron machine (Model 5542, Norwood, MA) to characterize the scaffolds and tissues mechanical properties. Samples were cut into 15 mm by 5 mm rectangular strips. Geometry data were imported in the Blue Hill mechanical testing software and samples were stretched to failure using a 10 N load cell to measure the reaction force. The samples were loaded at a 7 mm/min extension rate.

For the native pulmonary valve (PV) and aortic valve (AV) tissues, we measured the initial modulus (0–15% strain region; equivalent to the Young's modulus for a linear elastic material), transient modulus (~ 15–30% strain region) and the peak tangent modulus (i.e. the modulus in the steepest region of the stress–strain curve). In addition, the ultimate tensile strength (UTS; maximum stress at the peak point) and the strain-to-failure were measured for the native tissues. To ignore the plastic deformation in fibrous and tri-layered scaffolds, yield stress ($Y\sigma$) (stress at which the material begins to deform plastically) and yield strain ($Y\varepsilon$) (strain representing yield stress) were measured and considered in comparison study.

2.4. DNA, collagen and GAG assays

Samples (~2.5 mm by 2.5 mm) were cut from the cell-seeded scaffolds and weighed prior to the extraction of the ECM. The Sircol™ collagen assay kit (Biocolor Ltd., United Kingdom) was used as per the manufacturer's protocol to quantify the collagen content that was synthesized following the 2 and 4 weeks of cultivation. In order to extract the collagen, samples were placed in PCR tubes in 100 µl of extraction solution (0.5 M acetic acid and 1 mg/ml pepsin A in water) overnight on an orbital rocker at room temperature. GAGs were extracted utilizing the Sircol™ GAG assay kit (Biocolor Ltd., United Kingdom). Briefly, the samples were soaked in a 1 ml solution of 4 M guanidine-HCl and 0.5 M sodium acetate overnight at 2–8 °C. Following the extraction steps, ECM proteins (collagen and GAG content) were measured according to the protocol provided with the Sircol™ assay kits using a Genesys 20 spectrophotometer (Thermo Spectronic, Rochester, NY).

DNA content was quantified on fibrous, microfabricated and tri-layered scaffolds at each specific time point by using a PicoGreen dsDNA quantification kit (Invitrogen) per manufacturer's instruction using a Spectramax Gemini XS plate reader (Molecular Devices, Inc., Sunnyvale, CA). Samples (~2 mm by 2 mm) were first cut from the cell-seeded scaffolds and weighed. The samples were then incubated in microcentrifuge tubes with 1 ml of buffered papain solution at 0.125 mg/ml concentration (DNA extraction solution) for 16 h in a 60 °C water bath before performing the PicoGreen assay.

2.5. Histology and immunostaining

Samples were first fixed in 4% PFA for 30 min, then rinsed in PBS, and stored in 30% sucrose solution at 4 °C overnight. Then samples were then rinsed with PBS and embedded in OCT (Finetek). Cryosections of 10 µm were cut and stored at -20 °C. Sections were thawed for 30 min before performing hematoxylin and eosin (H&E) staining for general morphology. To visualize myofibroblast-like differentiation, cell-seeded scaffold sections were stained for alpha smooth muscle actin (α-SMA, mouse monoclonal 1A4, Dako) using immunofluorescence. Normal horse serum (4%) was used as a blocking solution. AlexaFluor 488 labeled secondary goat-anti-mouse (Invitrogen) served as the secondary antibody. Sections were coverslipped with DAPI-containing Vectashield mounting media to counterstain the nuclei. Images were taken with a Nikon Eclipse microscope equipped with a digital camera (Nikon Instruments, Melville, NY).

The cell-seeded scaffolds were prepared for nuclei and F-actin visualization. Samples were first rinsed in HBSS and then fixed in 10% neutral buffered formalin (Sigma) for 20 min. The samples were then allowed to incubate at room temperature for 2 h in 0.2% (v/v) Triton X-100 (Sigma) in *Hank's Balanced Salt Solution* (HBSS). The samples were then rinsed 3 times for 5 min each in 0.05% (v/v) Triton X-100 in HBSS and then blocked in 1% (w/v) bovine serum albumin (Sigma) and 0.05% (v/v) Triton X-100 in HBSS for 2 h. Once the blocking was complete, samples were incubated for 3 h in AlexaFluor 488-phalloidin 1:40 (v/v) dilution of stock solution in 1% (w/v) bovine serum albumin and 0.05% (v/v) Triton X-100 in HBSS. The scaffolds were then rinsed 5 times for 5 min each in HBSS and stored in the refrigerator overnight. The samples were then placed on glass slides and covered with a drop of Vectashield mounting media with DAPI (Vector Laboratories, Inc., Burlingame, CA) to counterstain cell nuclei.

2.6. Thrombogenicity assay

Human platelet rich plasma concentrates with approximately 1×10^6 platelets/ml was obtained from (ZenBio, Inc., NC). The platelets were spun down in 50 ml tubes (2700 rpm for 5 min). The pellet was resuspended in 500 µl of media which led to a concentration of about 1×10^8 platelets/ml. Scaffolds were washed with PBS and placed in 12 well plates. Samples were submerged in 400 µl of the platelet solution for 1 h on a rocker in an incubator. Following the soaking process, samples were washed with PBS, fixed in 10% formalin for 20 min and immunohistology was conducted as described above using anti-human CD41 (Invitrogen, Carlsbad, CA) (1:200 for 1 h at 37 °C) as a primary and anti-mouse Alexa 568 (1:40 for 1 h at room temperature) as a secondary antibody. Samples were stained with mouse anti-human CD41 (Invitrogen, Carlsbad, CA) (1:200 for 1 h at room

temperature). The samples were then washed and soaked in a solution of AlexaFluor 568 anti-mouse (1:40 for 1 h at room temperature).

2.7. Environmental scanning electron microscopy (ESEM) and confocal microscopy

Scaffolds were imaged at different magnifications (e.g. 50×, 100×) using an environmental scanning electron microscope (ESEM), SEMXL30 at low vacuum with a 32 kV accelerating voltage, 11 mm working distance. Immunohistology was visualized using a fluorescence microscope equipped with fluorescence camera (Axio Camera MRm) and manufactured ApoTome for depth imaging (Carl Zeiss Micro-Imaging, Gottingen, Germany).

2.8. Hemodynamic functionality

An *ex vivo* experiment was designed to test the scaffolds as a single leaflet replacement for PV. Fresh hearts were obtained from a local slaughter house and the right ventricles were cannulated and connected to a water reservoir. The right ventricle and the PA were cannulated and connected to different water reservoirs. The position of the fluid reservoir connected to the right ventricle (flow inlet) was chosen to provide a hydrostatic pressure similar to the systolic blood flow pressure at the position of the PV (about 30 mmHg). The pulmonary artery was connected to a second water reservoir through a tube, which provided 10 mmHg of pressure during diastole. Repetitive cycles of systole and diastole were manually generated by opening and closing the clamps attached to the inlet and outlet flow lines, with the implant visible during each cycle. The repetitive cycles of systole and diastole were manually controlled with the implant, visible during each cycle in real time. The scaffolds opening and closing was visualized using a surgical endoscope cannulated through the ventricles right beneath the PV position. Both single-layered fibrous scaffold and tri-layered scaffold were examined as PV single leaflet implants. Of note, the tri-layered scaffolds were sutured through the top and bottom fibrous layers to the PA to overcome the bending stiffness of tri-layered scaffolds inhibited the scaffolds natural movement during the test. This is in accordance with the native structure where the fibrosa and ventricularis layers are holding the scaffolds to the sinus wall.

2.9. Statistical analysis

Data is reported as mean \pm standard deviation (SD). For group comparisons, two-way ANOVA followed by Tukey's post-hoc tests were conducted. *P* values <0.05 were regarded to indicate significance ($*P < 0.05$, $**P < 0.01$ and $***P < 0.001$).

3. Results and discussion

Native tissues have complex 3D structures with several interconnected layers whose architecture dictates their mechanical characteristics and functionality, e.g. myocardial tissue featuring unique collagen architecture in the ventricular wall [51,52] or the fibrous layers of heart valve leaflets interconnected by the spongiosa middle layer. Anisotropic mechanical characteristic of the native tissue is one of the most important characteristics that directly influences their functionality. Essentially, the alignment of the fibers in the ECM determines the anisotropic characteristics of the tissues. For instance, dense collagen bundles and elastin network are oriented in the circumferential direction in myocardium and heart valve leaflets.

Consequently, these tissues are stiffer in the circumferential direction and more deformable in the radial. On the opposite, arterial blood vessels exhibit higher stiffness in the radial than in the circumferential direction to allow for compensation of the pulsatile blood flow without relevant deformation in the radial direction. These examples underline the importance of ECM architecture to define the mechanical characteristics and fulfill the functional requirements for different tissues. In this study, we attempt to fabricate a polymer-based tri-layered scaffold, which mimics the architecture and mechanical properties of the native heart valve for engineering a functional synthetic leaflet.

3.1. Scaffolds architecture and mechanics

The mechanical and architectural properties of scaffolds play a key role in cellular attachment, growth, alignment and consequently construct functionality. Previous studies have used different fabrication techniques, including micromolding and laser ablation, to create scaffolds that controlled cellular alignment in the engineered constructs while mimicking the anisotropic mechanics of the native tissues [48,51]. High resolution stereolithography [53] and replica molding were also used to fabricate non-woven scaffolds with appropriate pore shapes from poly(glycolic acid)/poly(L-lactic acid) (PGA/PLLA) [27]. Similar patterns were fabricated by laser microablation on PGS membranes for TEHV, exhibiting anisotropy due to the unique pore structure [28,48]. 3D layer assembly methods have also been used to generate 3D tissue constructs with appropriate anisotropic characteristics to guide tissue formation [51,53–55]. To mimic the fibrous structure of native tissues, electrospinning, wet spinning and melt spinning techniques have been used to create fibrous scaffolds [56]. Although recent technologies were successfully employed to engineer scaffolds with tunable mechanical properties, there have been limited number of studies on the control of mechanical and architectural characteristics of engineered scaffolds simultaneously to create functional tissue constructs.

3.1.1. Architecture—Tri-layered scaffolds, resembling native leaflet tissue layers, were fabricated using micromolding and electrospinning techniques. Using both micromolding and electrospinning techniques, enabled us to combine the respective strengths of the separate PGS and PCL materials in engineering different layers of 3D constructs. We then applied an automatic procedure to assemble the 3D construct with tunable architecture. A microfabricated PGS layer was first fabricated using a micromolding technique (Fig. 1A) [29] which resulted the formation of anisotropic PGS scaffolds with unique diamond pore geometries as shown in ESEM images in Fig. 2A–B. The low molecular weight of PGS impairs the ability to electrospinning pure PGS to create a fibrous structure. In comparison, PCL demonstrates higher mechanical stiffness and facilitates electrospinning procedure, but provides a less convenient environment for tissue cultures [23,57]. Therefore, mixing these polymers resulted in the formation structure with appropriate biocompatibility and mechanical strength analogous to the native leaflets.

Following PGS microfabrication, a directional electrospinning technique was used to generate aligned PGS–PCL fibers on either side of the microfabricated PGS scaffolds (Fig. 1B), resembling the layered structure of native leaflets (i.e. the *zona fibrosa*, the *zona spongiosa* and the *zona ventricularis*) (Fig. 1C). ESEM images of the aligned fibrous

PGS/PCL scaffolds and the cross-section of the tri-layered scaffold are depicted in Fig. 2C and D, respectively. The preferred direction of the fibers is parallel to the diamond long axis (PD) and XD is the orthogonal direction. As demonstrated by ESEM images at higher magnification (Fig. 2E–F), fibers, covering the microfabricated PGS layer, provided homogeneous interpenetrating porous networks in the structure of microfabricated PGS. This aligned network enhanced structural integrity of the tri-layered scaffold while preserving the anisotropic characteristic of the microfabricated PGS scaffolds. Various layer-by-layer assembly methods have been previously described to generate 3D porous structures by using manual stacking or even more complicated technologies to control the bonding procedure [29,51,54,58]. Here, we applied directional electrospinning between two parallel electrodes [59] to cover both sides of the microfabricated PGS layer with aligned PGS/PCL fibers. This process eliminated the use of complex stacking or any requirement for bonding technologies. In addition, we were able to achieve strong bonding between the layers by electrospinning directly on the plasma-treated microfabricated PGS scaffolds [54], which overcame layer delamination, mainly associated with layer-by-layer assembly techniques.

3.1.2. Mechanics—One of the fundamental requirements for tissue engineered scaffolds to serve in tissue engineering application is to provide mechanical support, while allowing for cellular in-growth and tissue formation during controlled scaffold degradation [16,23]. The effect of scaffold degradation on mechanical properties during tissue formation is an important factor that should be considered in clinical translation of tissue engineered constructs [23,29,48]. In the present study, we evaluated the degradation and changes in mechanical properties of the engineered scaffolds by incubating the unseeded constructs for 4 weeks in normal growth media (DMEM) at 37 °C. These scaffolds were 1) microfabricated PGS with diamond pores, 2) electrospun PGS/PCL fibers and 3) the tri-layered composite of microfabricated PGS surrounded by aligned fibers of electrospun PGS/PCL. Initial stiffness (tensile modulus; E), yield stress ($Y\sigma$) and yield strain ($Y\varepsilon$) (strain representing the plastic deformation) were measured at 0, 2 and 4 weeks of incubation (Fig. 3A–C). Lower stiffness and strength corresponding with higher elasticity (elongation) of the scaffolds were an indication of degradation and loss of mechanical strength (for tri-layered construct; $E_{\text{init.}}$: 3.02 ± 0.59 vs. $E_{4\text{wk}}$: 1.63 ± 0.36 MPa, ($P < 0.001$) $Y\varepsilon_{\text{init.}}$: 0.60 ± 0.08 vs. $Y\varepsilon_{4\text{wk}}$: 0.93 ± 0.15 ($P < 0.001$)). The highest rate of degradation was obtained with the microfabricated PGS scaffolds and the lowest for the fibrous PGS/PCL scaffolds (45% loss of stiffness for PGS scaffolds vs. 20% stiffness reduction for PGS/PCL fibrous scaffolds). These results are consistent with reported data from recent studies where PCL had a resident time *in vivo* on the order of 2–4 years whereas for PGS, it was weeks to months [47,60,61]. Cyclic tensile testing was performed to evaluate the reversible deformation and elastic characteristics of the tri-layered scaffolds compared to the native tissue leaflets (Fig. 3D). The energy loss of the fabricated tri-layered scaffolds was calculated about 32% which was comparable with the native leaflet's energy loss (27%) obtained following cyclic tensile loading test (up to 30% strain corresponding with native tissue strain amplitude during diastole). Representative stress–strain curves for fibrous PGS/PCL, microfabricated PGS scaffolds and tri-layered composites are depicted in Fig. 3E. Generally, for a material that experiences creep deformation following a linear trend in the stress–strain curve, the yield

stress would be the point that defines the strain amplitude at which the material deforms permanently and loses its deformation recovery ability [17,18]. Due to the presence of PCL, a highly plastic material, the tri-layered scaffolds and the fibrous PGS/PCL scaffolds underwent only small deformation up to a certain strain, termed the yield point [38]. Therefore, it is essential to consider only the linear portion of the stress–strain curve for the scaffolds that were able to recover during the stresses expected in the mammalian circulation. Consequently, for the scaffolds containing PCL, $Y\sigma$ and $Y\varepsilon$ were obtained as shown in Fig. 3E in addition to the initial tangent modulus (E). However, since PGS is an elastic material with linear stress–strain curves [43,48], the mechanical properties for microfabricated PGS scaffolds represented the initial tangent modulus (E), ultimate tensile strength (UTS) and strain to failure (ε_f). In addition, the different trend representative stress–strain curves for tri-layered composite containing aligned fibers and microfabricated PGS, depicted in both PD and XD directions, confirmed the anisotropic characteristic of the designed constructs (Fig. 3F) described in detail later.

Uniaxial tensile tests were performed to measure the mechanical properties of the native leaflets tissues (Fig. 4). Due to the crimped structure of collagen fibers in the native leaflets (both PV and AV), a non-linear trend of stress–strain curves were obtained for native leaflets. As shown in the graphs, less force was required initially to stretch the leaflets up to the point where the collagen fibers straightened (up to approximately 15–20% strain, initial region of the trend) (Fig. 4C). Once past this initial region and following the transient region, where the native collagen fibers were completely straight, higher force was required to further deform and stretch the leaflets, resulting in a sudden increase in the slope of the stress–strain curve (known as peak tangent) (Fig. 4C–D). The tangent modulus of native tissues in these three regions was also calculated and presented for AV and PV leaflets (in both circumferential and radial direction) in Fig. 4E–F, as are UTS and ε_f of the leaflets in Fig. 4G–H. These results demonstrate that leaflets are anisotropic as normal leaflet opening and closing during blood circulation are also dependent on the anisotropic mechanical characteristics of the leaflet [3,29]. These data were compared with engineered composite's anisotropy (Fig. 5A). Although the tri-layered scaffolds were highly anisotropic compared to existing TEHV constructs, the stiffness anisotropy obtained for these scaffolds ($E_{PD/XD}$: ~ 6) was lower than native PV values ($E_{CIRC/RAD}$: ~10). This finding could be due to the presence of dense collagen networks in AV and PV. However, the strength anisotropy of the fabricated tri-layered scaffolds was similar to the native tissue UTS anisotropy (UTS_{PD/XD}: 6 vs. UTS_{CIRC/RAD}: 6.3). A suture retention test was also performed on both native pulmonary artery (PA) and fibrous scaffolds and similar results were obtained for the sutured scaffolds and native tissues (Fig. 5B–C) where the sutured material ruptured at 0.85 ± 0.15 MPa while the native PA ruptured at 0.46 ± 0.21 MPa.

3.2. Tissue development

3.2.1. Mechanical properties following tissue formation—The fabricated scaffolds were seeded with sheep MSCs for up to 4 weeks and the mechanical properties of the cell-seeded tri-layered scaffolds were tested after 2 and 4 weeks of culture. A comparison between E , $Y\sigma$ and $Y\varepsilon$ of the tri-layered cell-seeded (Table 1) and unseeded scaffolds (Fig. 2A–C) showed that MSC-seeded scaffolds, following 4 weeks of cultivation, either retained

or exceeded the tensile modulus (E) and $Y\sigma$ obtained at the initial time of culture (In PD direction; $E_{\text{init.}}$: 3.02 ± 0.58 MPa vs. $E_{4\text{wk.}}$: 2.83 ± 0.32 MPa and $Y\sigma_{\text{init.}}$: 0.59 ± 0.15 MPa vs. $Y\sigma_{4\text{wk.}}$: 0.63 ± 0.09 MPa). The unseeded control scaffolds demonstrated ~20% (2wk) and ~35% (4wk) loss in E and ~5% (2wk and 4wk) decrease in $Y\sigma$ values with respect to initial properties. These changes in mechanical properties appeared to be compensated by progressive production of ECM proteins by the cells on the seeded constructs. These results are in line with the previous studies demonstrating the positive effect of collagen secretion on the scaffold stiffness [29,33].

The mechanical properties of tri-layered scaffolds, following 4 weeks of culture, were also compared to the mechanical characteristics of the native tissues (Fig. 6A–C). The stiffness of the transient region of the native tissue in stress–strain curve was considered for comparison based on the strain deformation and stress amplitude that native tissues experience *in vivo*. The initial stiffness of the material matched the transient stiffness of the native tissues, particularly for PV leaflets ($E_{\text{scaffolds/PD}}$: 2.83 ± 0.32 vs. $E_{\text{AV/CIRC}}$: 3.84 ± 0.06 and $E_{\text{PV/CIRC}}$: 2.55 ± 0.34 MPa) (Fig. 6A). Although, the scaffold's yield stress was lower than native tissue's UTS, that value is much higher than the stress that native tissue experience following 30% deformation in diastole (here defined as $\sigma_{30\%}$) (Fig. 6B). Physiologically, this is the stress/tension that native AV and PV experience during the opening and closing cycle and stress distribution on the tissue would not reach UTS levels, measured according to the blood flow pressure described in the equation (1) (calculation for PA):

$$(p.r=2t.T) \quad (1)$$

where P is the diastolic pressure of 20 mmHg, r is the PA diameter of 25 mm and t is the leaflet thickness of 300 μm [29]. Using this equation, the stress amplitude on the leaflet (tension, T) is ~65 kPa which is remarkably lower than the scaffold tolerance, $Y\sigma$ (0.63 ± 0.09 MPa) or even the native leaflets stress at 30% strain ($\sigma_{30\%}$) of native tissue (~400 kPa in circumferential direction measured from stress–strain graph) that has been compared with. During the normal circulation, the native leaflets stretch to about 25% strain during opening and closing. Thus, they are exposed to relatively low stress values, which can be derived from the stress–strain trend of native leaflets and the equation above (in the order of 0.1 MPa for PV and 0.25 MPa for AV). Tri-layered scaffolds were cultured with both sheep MSCs and VICs separately to assess the tissue formation and changes in the mechanical properties following 2 and 4 weeks cultivation. No significant differences were observed between the mechanical properties of MSC- vs. VIC-seeded scaffolds as shown in Fig. 6D.

3.2.2. Biochemical assays—To demonstrate the potential of our construct to support ECM formation, biochemical assays were performed following 1, 2, 3 and 4 weeks of MSC cultivation to measure DNA, collagen and GAG content in the scaffolds (Fig. 7A–C). We compared ECM protein deposition and DNA accumulation on fibrous PGS/PCL scaffolds, microfabricated PGS scaffolds, and the tri-layered composites with the values obtained from native AV and PV. The extracted total collagen, GAG and DNA from AV and PV did not differ considerably. However, mean collagen/DNA values (Supplementary IA) were slightly higher in mature AV compared to PV, which is consistent with the higher stiffness of AV

leaflets (Fig. 4). This could be due to the higher blood pressure in the left ventricular outflow tract in which the AV resides [29].

DNA content increased in scaffolds during the 4 weeks of culture, confirming MSC proliferation. The highest DNA content after 4 weeks of cultivation was found in the microfabricated scaffolds with large diamond-shaped pores. Interestingly, extracted DNA from tri-layered scaffolds matched the DNA content obtained from the native tissues (55 ± 9 vs. 58 ± 7 in AV and 51 ± 10 in PV) (Fig. 7A). These results suggest that the combination of fibers and micropores in tri-layered scaffolds may provide an appropriate environment for cell growth. To promote collagen synthesis, $82 \mu\text{g/ml}$ of L-ascorbic acid-2-phosphate was added to the culture media and collagen and GAG contents were quantified after 2 and 4 weeks of culture. Given the constant values of collagen and GAG contents within the single layer fibrous scaffolds from week 2 to week 4, we concluded that fibers alone did not support adequate tissue formation. ECM extraction from tri-layered scaffolds indicated that collagen and GAG content increased considerably with time ($P < 0.001$ for collagen production reported in each time point, and $P < 0.05$ for GAG production between time zero and week 2 and 4) (Fig. 7B–C). GAG content extracted from tri-layered scaffolds at week 4, as opposed to single fibrous and microfabricated scaffolds, was similar to those obtained from native tissue ECM extraction which could be due to the similarity between the microstructure of the fabricated composite and the native tissue. Collagen content extracted from tri-layered scaffolds ($1154 \pm 226 \mu\text{g/g}$ wet weight) was considerably higher than our previously reported data on double layer PGS microfabricated scaffolds seeded with VICs (681 ± 63 and $615 \pm 56 \mu\text{g/g}$ wet weight, for scaffolds seeded with aortic VICs and pulmonary VICs respectively) [28]. Single layer microfabricated PGS scaffold collagen content was similar to previous data obtained for laser microfabricated PGS scaffolds seeded with rat fibroblasts ($736 \pm 193 \mu\text{g/g}$ wet weight) [28] or values reported by Engelmayr et al. based on smooth muscle cell-seeded scaffolds ($546 \pm 111 \mu\text{g/g}$ wet weight for the statically incubated samples and $893 \pm 133 \mu\text{g/g}$ wet weight for the cyclically flexed samples). However, the collagen concentration extracted from engineered tissues was far lower than those measured in native sheep porcine AV and PV. The reported values are consistent with recently measured collagen concentration of porcine AV and PV using the same collagen assay protocol [62]. Considering the previous study results and current results (4 weeks cultivation of engineered scaffolds particularly in static condition), collagen formation is considerable but yet incomparable with native leaflet collagen concentration.

Prior studies have demonstrated that scaffold structure and porosity affect cell–cell and cell–matrix interactions. Higher porosity and pore interconnectivity provide adequate surface area for cell growth and ECM generation [51]. A relatively lower amount of DNA and higher amount of collagen and GAG extracted from the tri-layered scaffolds resulted in higher collagen/DNA and GAG/DNA values for the composite scaffolds (Supplementary IA–B). This confirmed the hypothesis that the scaffold's architecture affects the cellular functionality in terms of ECM deposition and tissue formation [27,29,51,54]. This finding could indicate that cell signaling in tri-layered scaffolds switched from a state of proliferation to ECM deposition. The underlying cause might have been the structural arrangement of the tri-layered scaffold, which resembles native heart valves. The

GAG/DNA ratios were also comparable with those of native tissues (Supplementary IA), but collagen/DNA values were lower than values obtained for native tissues as described above. A comparison between DNA content and ECM protein deposition on tri-layered scaffolds seeded with sheep MSCs and sheep VICs did not demonstrate considerable differences except for an increase in GAG content (obtained after 4wk culture) from VIC-seeded scaffolds (Supplementary II).

3.3. ESEM and immunostaining-histology

The presence of cells and deposited ECM within the pores of each scaffold was confirmed by ESEM and H&E staining (Fig. 7D–I). To ensure cell migration and tissue formation into the middle layer of the tri-layered scaffolds, ESEM images were taken from the cross-sections of the tri-layered scaffolds, demonstrating that cells formed layers within the 3D structure of the composite scaffolds (Fig. 7F–G). In addition, the majority of the fibers and diamond pores were mostly filled with cells and ECM proteins as shown in Fig. 7D–E. Differences between the native tissue sections and cultivated engineered tissues (Fig. 7H–I), with respect to the presence of ECM could be related to the difference of collagen concentration in engineered tissues vs. native tissues as confirmed by the collagen assays. In addition, delamination of the layers during the cryo-sectioning process could also result in loss of cells and tissues (Fig. 7H–I).

VICs are quiescent *in vivo* unless activated to trans-differentiate into myofibroblast-like cells, hallmarked by the expression α -SMA [63] and matrix remodeling enzymes (MMPs, TIMPs, and cathepsins) [13]. The remodeling potential of cells seeded onto our scaffold *in vitro* was observed by positive staining for α -SMA, indicative of a myofibroblast-like differentiation (Fig. 8A). The network of cells and oriented collagen fibers are important in dictating the mechanical properties of native heart valve leaflets and TEHVs [16,17,27,64]. Cell morphology, alignment and orientation were assessed within the scaffolds after 4 weeks of culture by immunostaining for F-actin and DAPI. On the tri-layered scaffold architecture, MSCs aligned in the preferred direction (toward the fiber direction on the surfaces and the long axis of diamond pores in the middle layer) as assessed by immunostaining for F-actin and DAPI (Fig. 8B–C). The cells were highly aligned along the direction of aligned fibers and along the long dimension of the diamond pores in the middle layer [29]. Considering the collagen and elastin fiber formation in the direction of aligned cells, we were able to conclude that the scaffold anisotropy was preserved (as reflected in the mechanical properties of cell-seeded scaffolds as well) during the degradation of the construct.

One of the critical challenges in using synthetic or biological scaffolds for TEHV is the risk of thrombus formation on the scaffolds, which limits the use of bare scaffolds for implantation. To overcome this problem, previous attempts were made to endothelialize the surface of scaffolds prior to implantation [7,30]. Here, we conducted thrombogenicity assays on our unseeded tri-layered scaffolds based on previously described procedures to investigate the thrombus formation on the fabricated scaffolds [65]. Comparing the images obtained from gelatin coated plates (positive control samples) with tri-layered and fibrous scaffolds, only a minimal number of platelets (red dots) attached to the surfaces of the

scaffolds which suggested that the fabricated scaffolds were not prone to thrombus formation (Fig. 8D).

3.4. Functionality test

To evaluate the ability of tri-layered scaffolds to open and close at the site of action, we designed an *ex vivo* experiment to test the potential of these scaffolds as a leaflet replacement in the PV position of isolated fresh pig hearts (Fig. 9A–C). The pressure in the system was controlled and maintained at 30 mmHg–10 mmHg for representing systolic and diastolic pressure respectively by adjusting the water reservoir position. Both single-layered fibrous scaffolds and tri-layered scaffolds were examined as PV single leaflet implants. Tri-layered scaffolds had adequate diastolic leaflet coaptation, whereas single-layered fibrous scaffolds coated incompletely during diastole observed from endoscopic video images (Supplementary III). This observation could be due to the lower bending stiffness of the thin fibrous structure.

Supplementary video related to this article can be found at <http://dx.doi.org/10.1016/j.biomaterials.2014.04.039>.

4. Conclusion

In an attempt to engineer functional TEHV constructs, a reasonable initial target is to match the native tissue properties such as mechanical stiffness and anisotropy and cellular and ECM composition and organization. In this study, we developed a biomimetic heart valve tissue engineered construct, which could eliminate the limitations of previously fabricated scaffolds for heart valve regeneration. In particular, by combining a micromolding technology and a directional electrospinning technique, we fabricated a tri-layered scaffold, comprised of diamond-shaped pores and aligned PGS/PCL fibers on the surfaces to emulate the anisotropy and mechanical properties of native leaflets. Both seeded and unseeded scaffolds were mechanically tested and the engineered tissue constructs were characterized for DNA, collagen and GAG content. These scaffolds structurally and mechanically mimicked a number of features of the native leaflet tissue, while providing appropriate support and environmental cues for ECM deposition and cell proliferation. The engineered scaffolds were also able to guide the cellular arrangement due to their unique structure corresponding to native tissue architecture.

Supplementary Material

Refer to Web version on PubMed Central for supplementary material.

Acknowledgments

The authors acknowledge funding from the National Science Foundation Career Award (DMR 0847287), the Office of Naval Research Young Investigator Award, the National Institutes of Health (HL092836, DE019024, EB012597, AR057837, DE021468, HL099073), and the German Heart Foundation (S/04/12). Authors would like to thank Alexander Cubberly for his great help with tissue culturing, Jen Piselli for her help with the schematic and Dr. Kolewe for his scientific comments on the paper.

Appendix A. Supplementary data

Supplementary data related to this article can be found at <http://dx.doi.org/10.1016/j.biomaterials.2014.04.039>.

References

1. Cannegieter S, Rosendaal F, Briet E. Thromboembolic and bleeding complications in patients with mechanical heart valve prostheses. *Circulation*. 1994; 89:635–41. [PubMed: 8313552]
2. Hammermeister KE, Sethi GK, Henderson WG, Oprian C, Kim T, Rahimtoola S. A comparison of outcomes in men 11 years after heart-valve replacement with a mechanical valve or bioprosthesis. *N Engl J Med*. 1993; 328:1289–96. [PubMed: 8469251]
3. Sacks MS, Schoen FJ, Mayer JE. Bioengineering challenges for heart valve tissue engineering. *Annu Rev Biomed Eng*. 2009; 11:289–313. [PubMed: 19413511]
4. Sewell-Loftin M, Chun YW, Khademhosseini A, Merryman WD. EMT-inducing biomaterials for heart valve engineering: taking cues from developmental biology. *J Cardiovasc Transl Res*. 2011; 4:658–71. [PubMed: 21751069]
5. Schoen FJ, Levy RJ. Calcification of tissue heart valve substitutes: progress toward understanding and prevention. *Ann Thorac Surg*. 2005; 79:1072–80. [PubMed: 15734452]
6. Cebotari S, Lichtenberg A, Tudorache I, Hilfiker A, Mertsching H, Leyh R, et al. Clinical application of tissue engineered human heart valves using autologous progenitor cells. *Circulation*. 2006; 114:I-132–7. [PubMed: 16820562]
7. Gottlieb D, Kunal T, Emani S, Aikawa E, Brown DW, Powell AJ, et al. In vivo monitoring of function of autologous engineered pulmonary valve. *J Thorac Cardiovasc Surg*. 2010; 139:723–31. [PubMed: 20176213]
8. Hoerstrup SP, Sodian R, Daebritz S, Wang J, Bacha EA, Martin DP, et al. Functional living trileaflet heart valves grown in vitro. *Circulation*. 2000; 102:III-44–9. [PubMed: 11082361]
9. Mol A, Driessen NJ, Rutten MC, Hoerstrup SP, Bouten CV, Baaijens FP. Tissue engineering of human heart valve leaflets: a novel bioreactor for a strain-based conditioning approach. *Ann Biomed Eng*. 2005; 33:1778–88. [PubMed: 16389526]
10. Robinson PS, Johnson SL, Evans MC, Barocas VH, Tranquillo RT. Functional tissue-engineered valves from cell-remodeled fibrin with commissural alignment of cell-produced collagen. *Tissue Eng Part A*. 2008; 14:83–95. [PubMed: 18333807]
11. Shinoka T, Breuer CK, Tanel RE, Zund G, Miura T, Ma PX, et al. Tissue engineering heart valves: valve leaflet replacement study in a lamb model. *Ann Thorac Surg*. 1995; 60:S513–6. [PubMed: 8604922]
12. Vesely I. Heart valve tissue engineering. *Circ Res*. 2005; 97:743–55. [PubMed: 16224074]
13. Schoen FJ. Evolving concepts of cardiac valve dynamics: the continuum of development, functional structure, pathobiology, and tissue engineering. *Circulation*. 2008; 118:1864–80. [PubMed: 18955677]
14. Kunzelman KS, Cochran RP, Murphree SS, Ring WS, Verrier ED, Eberhart RC. Differential collagen distribution in the mitral valve and its influence on biomechanical behaviour. *J Heart Valve Dis*. 1993; 2:236–44. [PubMed: 8261162]
15. Sacks MS, David Merryman W, Schmidt DE. On the biomechanics of heart valve function. *J Biomech*. 2009; 42:1804–24. [PubMed: 19540499]
16. Sacks MS, Yoganathan AP. Heart valve function: a biomechanical perspective. *Philos Trans R Soc Lond B Biol Sci*. 2007; 362:1369–91. [PubMed: 17588873]
17. Stella JA, Sacks MS. On the biaxial mechanical properties of the layers of the aortic valve leaflet. *J Biomech Eng*. 2007; 129:757–66. [PubMed: 17887902]
18. Weinberg EJ, Kaazempur-Mofrad MR. On the constitutive models for heart valve leaflet mechanics. *Cardiovasc Eng*. 2005; 5:37–43.

19. Alavi SH, Ruiz V, Krasieva T, Botvinick EL, Kheradvar A. Characterizing the collagen fiber orientation in pericardial leaflets under mechanical loading conditions. *Ann Biomed Eng.* 2013; 41:547–61. [PubMed: 23180029]
20. Brody S, Pandit A. Approaches to heart valve tissue engineering scaffold design. *J Biomed Mater Res B Appl Biomater.* 2007; 83:16–43. [PubMed: 17318822]
21. Annabi N, Mithieux SM, Camci-Unal G, Dokmeci MR, Weiss AS, Khademhosseini A. Elastomeric recombinant protein-based biomaterials. *Biochem Eng.* 2013; 77:110–8.
22. Annabi N, Tsang K, Mithieux SM, Nikkhah M, Ameri A, Khademhosseini A, et al. Highly elastic micropatterned hydrogel for engineering functional cardiac tissue. *Adv Funct Mater.* 2013; 18:39–49.
23. Sant S, Iyer D, Gaharwar A, Patel A, Khademhosseini A. Effect of biodegradation and de novo matrix synthesis on the mechanical properties of VIC-seeded PGS-PCL scaffolds. *Acta Biomater.* 2012; 9:5963–73. [PubMed: 23168222]
24. Hockaday L, Kang K, Colangelo N, Cheung P, Duan B, Malone E, et al. Rapid 3D printing of anatomically accurate and mechanically heterogeneous aortic valve hydrogel scaffolds. *Biofabrication.* 2012; 4:035005. [PubMed: 22914604]
25. Williams C, Johnson SL, Robinson PS, Tranquillo RT. Cell sourcing and culture conditions for fibrin-based valve constructs. *Tissue Eng.* 2006; 12:1489–502. [PubMed: 16846346]
26. Duan B, Hockaday LA, Kang KH, Butcher JT. 3D bioprinting of heterogeneous aortic valve conduits with alginate/gelatin hydrogels. *J Biomed Mater Res A.* 2013; 101:1255–64. [PubMed: 23015540]
27. Engelmayer GC Jr, Papworth GD, Watkins SC, Mayer JE Jr, Sacks MS. Guidance of engineered tissue collagen orientation by large-scale scaffold microstructures. *J Biomech.* 2006; 39:1819–31. [PubMed: 16043186]
28. Masoumi N, Jean A, Zugates JT, Johnson KL, Engelmayer GC Jr. Laser microfabricated poly(glycerol sebacate) scaffolds for heart valve tissue engineering. *J Biomed Mater Res A.* 2013; 101:104–14. [PubMed: 22826211]
29. Masoumi N, Johnson KL, Howell MC, Engelmayer GC Jr. Valvular interstitial cell seeded poly(glycerol sebacate) scaffolds: toward a biomimetic in vitro model for heart valve tissue engineering. *Acta Biomater.* 2013; 9:5974–88. [PubMed: 23295404]
30. Weber B, Dijkman PE, Scherman J, Sanders B, Emmert MY, Grünenfelder J, et al. Off-the-shelf human decellularized tissue-engineered heart valves in a non-human primate model. *Biomaterials.* 2013; 34:7269–80. [PubMed: 23810254]
31. Berry JL, Steen JA, Koudy Williams J, Jordan JE, Atala A, Yoo JJ. Bioreactors for development of tissue engineered heart valves. *Ann Biomed Eng.* 2010; 38:3272–9. [PubMed: 20820920]
32. Engelmayer GC Jr, Sacks MS. A structural model for the flexural mechanics of nonwoven tissue engineering scaffolds. *J Biomech Eng.* 2006; 128:610–22. [PubMed: 16813453]
33. Engelmayer GC Jr, Rabkin E, Sutherland FW, Schoen FJ, Mayer JE Jr, Sacks MS. The independent role of cyclic flexure in the early in vitro development of an engineered heart valve tissue. *Biomaterials.* 2005; 26:175–87. [PubMed: 15207464]
34. Sutherland FW, Perry TE, Nasser BA, Wang J, Kaushal S, Guleserian KJ, et al. Advances in the mechanisms of cell delivery to cardiovascular scaffolds: comparison of two rotating cell culture systems. *ASAIO J.* 2002; 48:346–9. [PubMed: 12141461]
35. Merryman WD, Youn I, Lukoff HD, Krueger PM, Guilak F, Hopkins RA, et al. Correlation between heart valve interstitial cell stiffness and transvalvular pressure: implications for collagen biosynthesis. *Am J Physiol Heart Circ Physiol.* 2006; 290:H224–31. [PubMed: 16126816]
36. Engelmayer GC Jr, Sacks MS. Prediction of extracellular matrix stiffness in engineered heart valve tissues based on nonwoven scaffolds. *Biomech Model Mechanobiol.* 2008; 7:309–21. [PubMed: 17713801]
37. Annabi N, Mithieux SM, Weiss AS, Dehghani F. Cross-linked open-pore elastic hydrogels based on tropoelastin, elastin and high pressure CO₂. *Biomaterials.* 2010; 31:1655–65. [PubMed: 19969349]

38. Sant S, Hwang CM, Lee SH, Khademhosseini A. Hybrid PGS–PCL microfibrinous scaffolds with improved mechanical and biological properties. *J Tissue Eng Regen Med*. 2011; 5:283–91. [PubMed: 20669260]
39. Benton JA, DeForest CA, Vivekanandan V, Anseth KS. Photocrosslinking of gelatin macromers to synthesize porous hydrogels that promote valvular interstitial cell function. *Tissue Eng Part A*. 2009; 15:3221–30. [PubMed: 19374488]
40. Bruggeman JP, Bettinger CJ, Nijst CL, Kohane DS, Langer R. Biodegradable xylitol-based polymers. *Adv Mater*. 2008; 20:1922–7.
41. Guan J, Sacks MS, Beckman EJ, Wagner WR. Biodegradable poly(ether ester urethane) urea elastomers based on poly(ether ester) triblock copolymers and putrescine: synthesis, characterization and cytocompatibility. *Biomaterials*. 2004; 25:85–96. [PubMed: 14580912]
42. Pereira MJN, Ouyang B, Sundback CA, Lang N, Friehs I, Mureli S, et al. A highly tunable biocompatible and multifunctional biodegradable elastomer. *Adv Mater*. 2013; 25:1209–15. [PubMed: 23239051]
43. Wang Y, Ameer GA, Sheppard BJ, Langer R. A tough biodegradable elastomer. *Nat Biotechnol*. 2002; 20:602–6. [PubMed: 12042865]
44. Annabi N, Mithieux SM, Zorlutuna P, Camci-Unal G, Weiss AS, Khademhosseini A. Engineered cell-laden human protein-based elastomer. *Biomaterials*. 2013; 34:5496–505. [PubMed: 23639533]
45. Annabi N, Tamayol A, Uquillas JA, Akbari M, Bertassoni LE, Cha C, et al. 25th Anniversary article: rational design and applications of hydrogels in regenerative medicine. *Adv Mater*. 2014; 26:85–124. [PubMed: 24741694]
46. Martin C, Sun W. Biomechanical characterization of aortic valve tissue in humans and common animal models. *J Biomed Mater Res Part A*. 2012; 100:1591–9.
47. Wang Y, Kim YM, Langer R. In vivo degradation characteristics of poly(glycerol sebacate). *J Biomed Mater Res A*. 2003; 66:192–7. [PubMed: 12833446]
48. Engelmayr GC, Cheng M, Bettinger CJ, Borenstein JT, Langer R, Freed LE. Accordion-like honeycombs for tissue engineering of cardiac anisotropy. *Nat Mater*. 2008; 7:1003–10. [PubMed: 18978786]
49. Pomerantseva I, Krebs N, Hart A, Neville CM, Huang AY, Sundback CA. Degradation behavior of poly(glycerol sebacate). *J Biomed Mater Res A*. 2009; 91:1038–47. [PubMed: 19107788]
50. Masoumi, N.; Larson, BL.; Annabi, N.; Kharaziha, M.; Zamanian, B.; Shaper, KS., et al. Electropun PGS: PCL microfibers align human valvular interstitial cells and provide tunable scaffold anisotropy. *Adv Health Mater*. 2014. <http://dx.doi.org/10.1002/adhm.201300505>
51. Kolewe ME, Park H, Gray C, Ye X, Langer R, Freed LE. 3D structural patterns in scalable, elastomeric scaffolds guide engineered tissue architecture. *Adv Mater*. 2013; 25:4459–65. [PubMed: 23765688]
52. LeGrice IJ, Smaill B, Chai L, Edgar S, Gavin J, Hunter PJ. Laminar structure of the heart: ventricular myocyte arrangement and connective tissue architecture in the dog. *Am J Physiol*. 1995; 269:H571–82. [PubMed: 7653621]
53. Gauvin R, Chen Y-C, Lee JW, Soman P, Zorlutuna P, Nichol JW, et al. Microfabrication of complex porous tissue engineering scaffolds using 3D projection stereolithography. *Biomaterials*. 2012; 33:3824–34. [PubMed: 22365811]
54. Park H, Larson BL, Guillemette MD, Jain SR, Hua C, Engelmayr GC Jr, et al. The significance of pore microarchitecture in a multi-layered elastomeric scaffold for contractile cardiac muscle constructs. *Biomaterials*. 2011; 32:1856–64. [PubMed: 21144580]
55. Fozdar DY, Soman P, Lee JW, Han LH, Chen S. Three-dimensional polymer constructs exhibiting a tunable negative Poisson's ratio. *Adv Funct Mater*. 2011; 21:2712–20. [PubMed: 21841943]
56. Tamayol A, Akbari M, Annabi N, Paul A, Khademhosseini A, Juncker D. Fiber-based tissue engineering: progress, challenges, and opportunities. *Biotechnol Adv*. 2012; 31:669–87. [PubMed: 23195284]
57. Sant S, Khademhosseini A. Fabrication and characterization of tough elastomeric fibrous scaffolds for tissue engineering applications. *Conf Proc IEEE Eng Med Biol Soc*. 2010; 2010:3546–8. [PubMed: 21096824]

58. Ryu W, Min SW, Hammerick KE, Vyakarnam M, Greco RS, Prinz FB, et al. The construction of three-dimensional micro-fluidic scaffolds of biodegradable polymers by solvent vapor based bonding of micro-molded layers. *Biomaterials*. 2007; 28:1174–84. [PubMed: 17126395]
59. Kharaziha M, Nikkhah M, Shin S-R, Annabi N, Masoumi N, Gaharwar AK, et al. PGS: gelatin nanofibrous scaffolds with tunable mechanical and structural properties for engineering cardiac tissues. *Biomaterials*. 2013; 34:6355–66. [PubMed: 23747008]
60. Lam CX, Savalani MM, Teoh S-H, Hutmacher DW. Dynamics of in vitro polymer degradation of polycaprolactone-based scaffolds: accelerated versus simulated physiological conditions. *Biomed Mater*. 2008; 3:034108. [PubMed: 18689929]
61. Sundback CA, Shyu JY, Wang Y, Faquin WC, Langer RS, Vacanti JP, et al. Biocompatibility analysis of poly(glycerol sebacate) as a nerve guide material. *Biomaterials*. 2005; 26:5454–64. [PubMed: 15860202]
62. Huang H-YS, Liao J, Sacks MS. In-situ deformation of the aortic valve interstitial cell nucleus under diastolic loading. *J Biomed Eng*. 2007; 129:880–9.
63. Rabkin E, Aikawa M, Stone JR, Fukumoto Y, Libby P, Schoen FJ. Activated interstitial myofibroblasts express catabolic enzymes and mediate matrix remodeling in myxomatous heart valves. *Circulation*. 2001; 104:2525–32. [PubMed: 11714645]
64. Joyce EM, Liao J, Schoen FJ, Mayer JE Jr, Sacks MS. Functional collagen fiber architecture of the pulmonary heart valve cusp. *Ann Thorac Surg*. 2009; 87:1240–9. [PubMed: 19324159]
65. Zhang X, Xu Y, Thomas V, Bellis SL, Vohra YK. Engineering an antiplatelet adhesion layer on an electrospun scaffold using porcine endothelial progenitor cells. *J Biomed Mater Res A*. 2011; 97:145–51. [PubMed: 21370444]

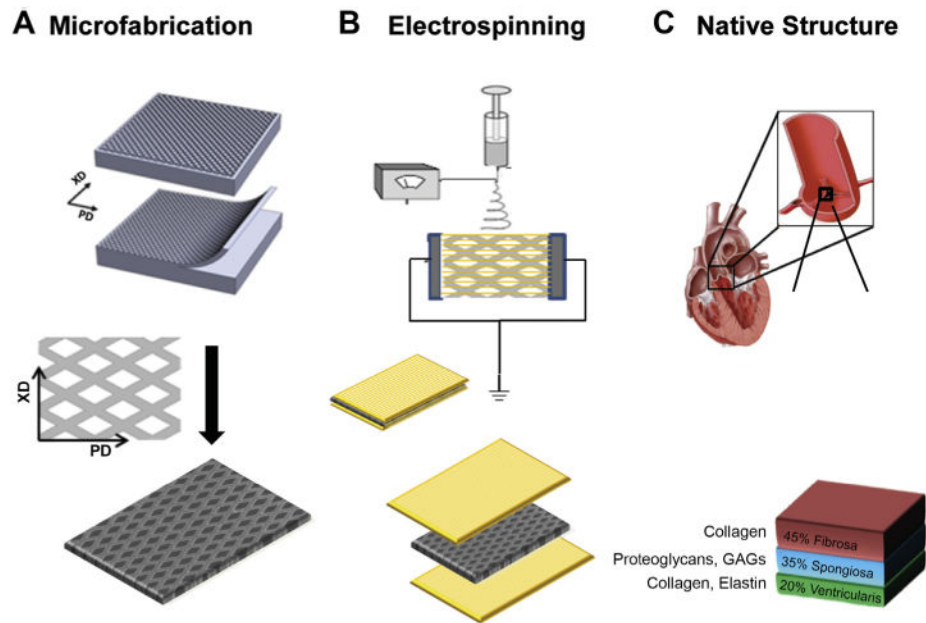


Fig. 1. Schematic diagrams of the scaffold fabrication process. (A) To form microfabricate PGS scaffold, PGS solution was first poured onto a ceramic mold containing diamond patterns and cured at 1600 °C for 8 h. The surface layer was then delaminated from the mold and rinsed with PBS to remove the ceramic pieces from the microfabricated scaffolds. (B) To form the tri-layered composite scaffold, the PGS sheet was then placed between two aluminum electrodes and connected to a ground. PGS/PCL fibers were electrospun on either side of the PGS layer. (C) The composite resembles the structure of heart valve leaflets, consisting of three interconnected layers; the *zona fibrosa*, the *zona spongiosa* and the *zona ventricularis*, with collagen, GAGs and elastin representing the predominant ECM component in these three respective layers.

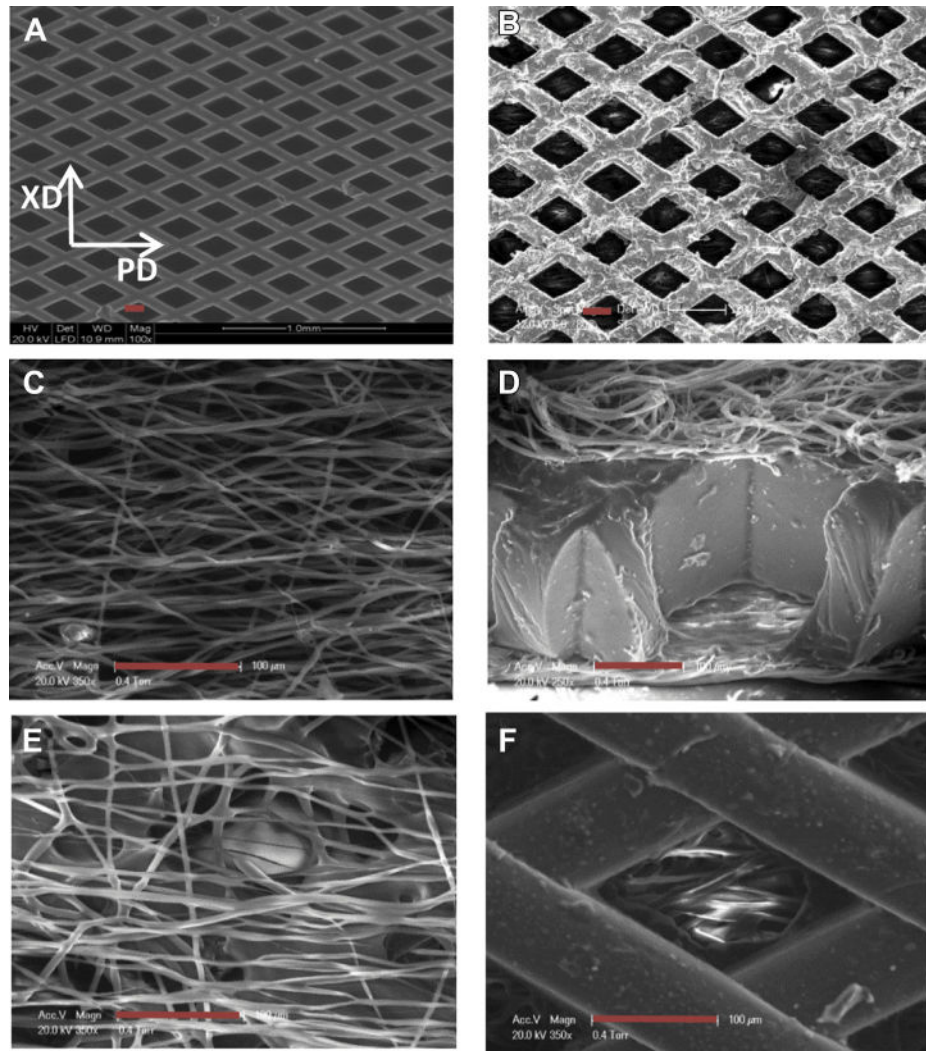


Fig. 2. Microstructures of the fabricated scaffold. ESEM micrographs of microfabricated PGS scaffolds (A) without and (B) with an aligned fibrous layer underneath. (C) Aligned fibers of PGS/PCL scaffolds and (D) cross-section of tri-layered scaffolds comprised of a PGS layer and fibers on both surfaces. (E) Aligned fibers on top and (F) bottom of a diamond pore (scale bars: 100 μm).

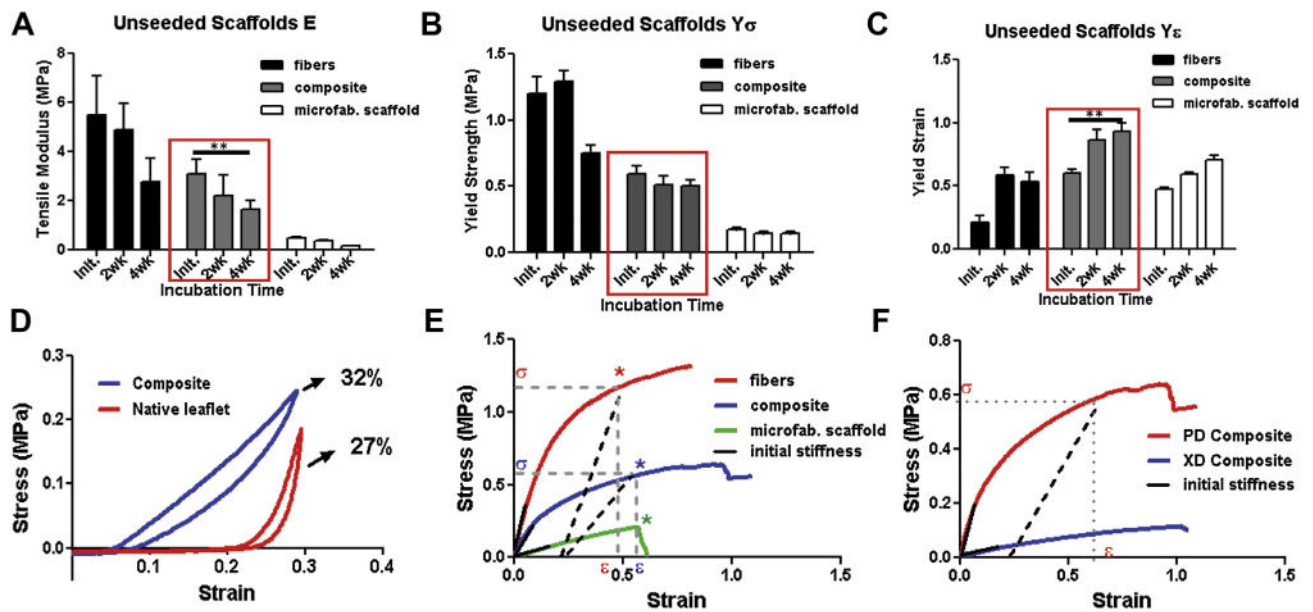


Fig. 3. Uniaxial mechanical testing of unseeded and seeded scaffolds. (A–C) Uniaxial tensile mechanical properties of unseeded scaffolds in PD directions, tested following 4 weeks of soaking in media, demonstrating that (A) E and (B) UTS decreased whereas (C) ϵ_f increased following scaffolds' degradation with time. (D) Representative cyclic stress–strain curves for tri-layered composite scaffold and native tissue are presented to compare the energy loss during 4 repetitive cyclic tests. (E) Representative stress–strain curves of fibrous, microfabricated PGS scaffold, and tri-layered composite scaffold in the PD direction. A creep deformation was observed in fibrous and tri-layered scaffolds following 25–50% strain (slightly less for tri-layered scaffold) while PGS showed a completely elastic behavior with linear trend in the stress–strain curve (the initial stiffness E , $Y\sigma$ and $Y\epsilon$ were obtained as shown in graphs). (F) Representative stress–strain curves of tri-layered scaffolds presented in PD and XD directions, indicating the anisotropic properties of the construct. (** $P < 0.01$).

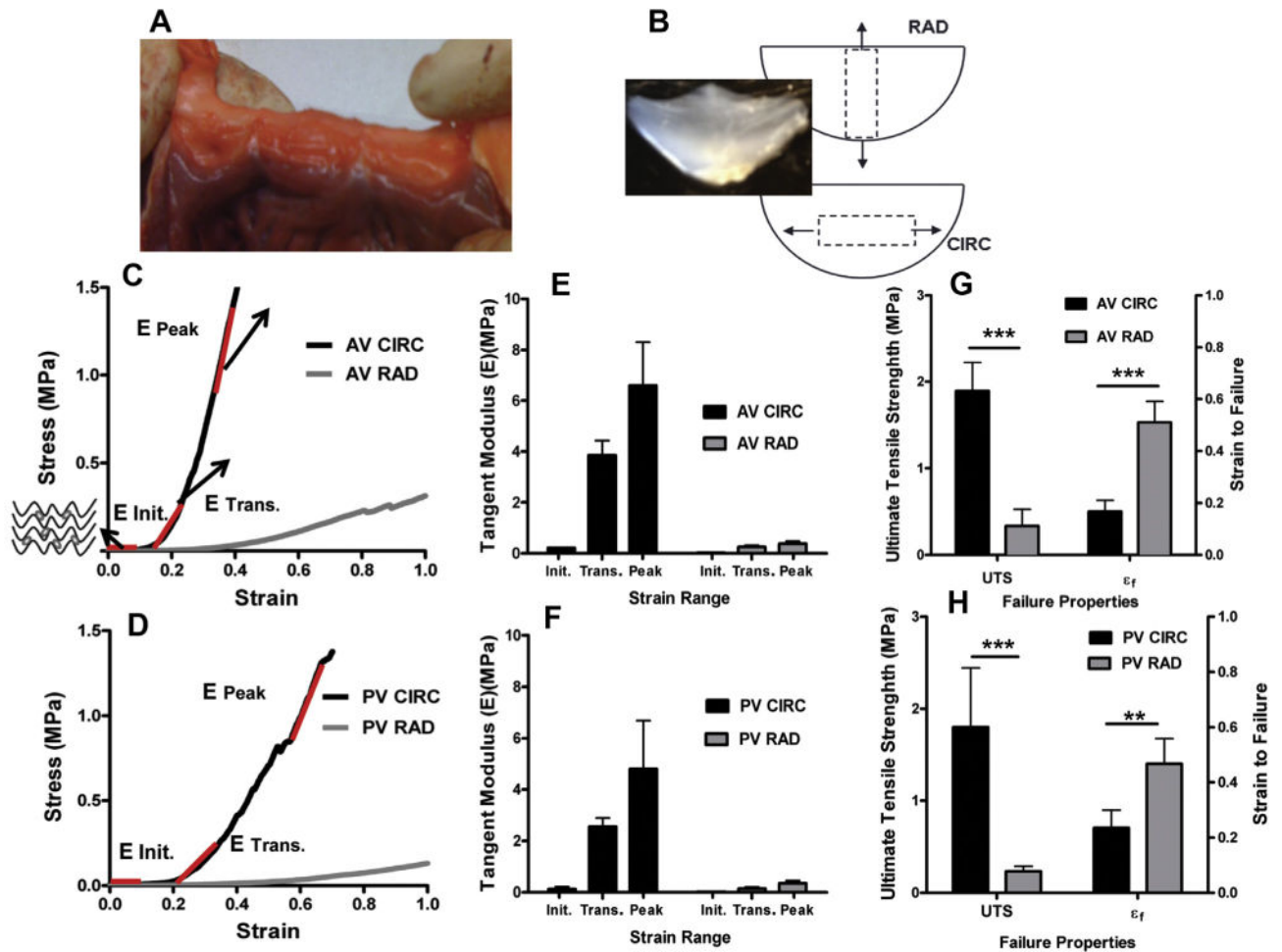


Fig. 4.

Mechanical properties of native AV and PV. Native tissue specimens were cut from explanted sheep leaflets in (A) circumferential (CIRC) and (B) radial (RAD) directions. Representative stress–strain curves of native (C) AV and (D) PV leaflets illustrate the non-linear, anisotropic mechanical response of the tissues. (E–F) Tangent moduli E were calculated for AV/PV in three regions and presented as initial ($E_{init.}$), transient ($E_{trans.}$) and peak tangent ($E_{peak.}$) moduli. Both orientation and strain range were statistically significant for tangent E . (G, H) Ultimate tensile strength (UTS) and strain-to-failure (ϵ_f) for the (G) AV and (H) PV leaflets. The UTS in the RAD direction were significantly less than those in the CIRC direction while the leaflets were more deformable in the RAD direction. Therefore, ϵ_f values were significantly greater in the RAD direction vs. the CIRC direction. (** $P < 0.01$ and *** $P < 0.001$).

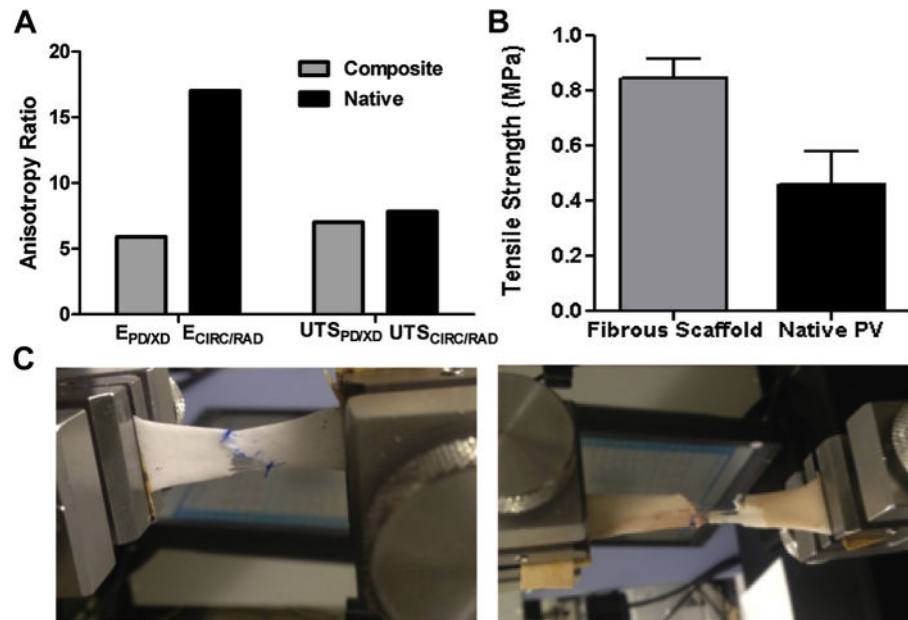


Fig. 5. Anisotropy and suture test of the tri-layered scaffolds vs. native tissues. (A) Comparison between the scaffold anisotropy (defined as ratio of stiffness and UTS in PD and XD directions), and the native leaflet's anisotropy (defined as ratio of stiffness and UTS in CIR and RAD directions). (B–C) Suture retention tests on fabricated scaffolds and the native tissues, demonstrated similar results.

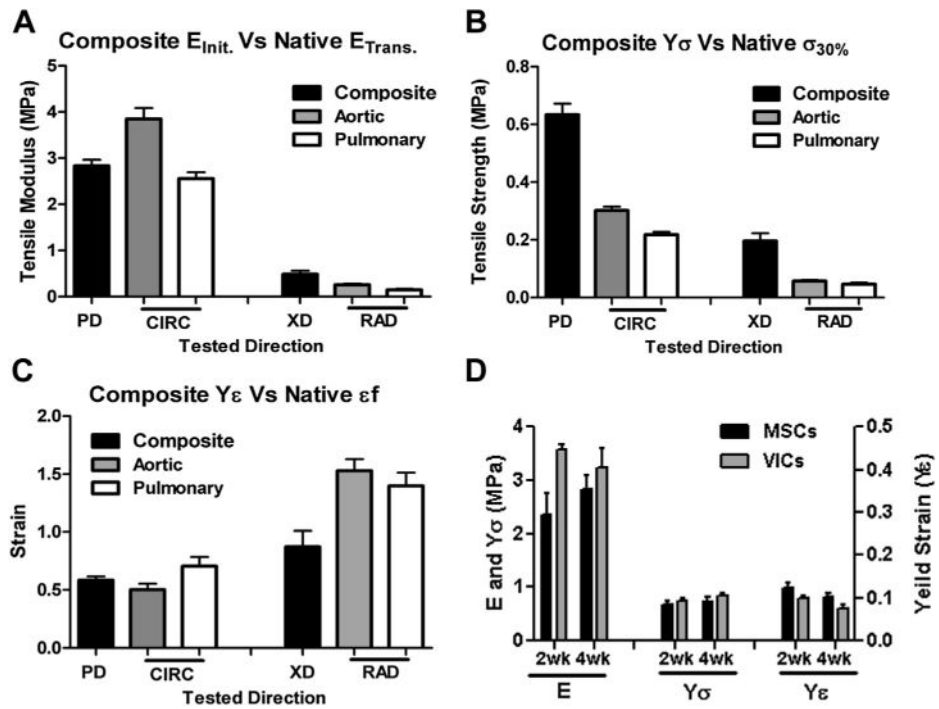


Fig. 6.

Mechanical properties of tri-layered scaffolds compared to native heart valve leaflet mechanics. (A–C) The tri-layered scaffold mechanical properties (i.e. E_{init} , Y_{σ} and Y_{ϵ}) assessed in both PD and XD directions following 4 weeks of culturing, and compared with the native tissue stiffness in transient region; $E_{trans.}$, stress at 30% deformation ($\sigma_{30\%}$) and strain to failure respectively. (D) Mechanical characteristics of sheep MSC- and VIC-seeded tri-layered scaffolds following 2 and 4 weeks culture, indicating no significant differences between the samples.

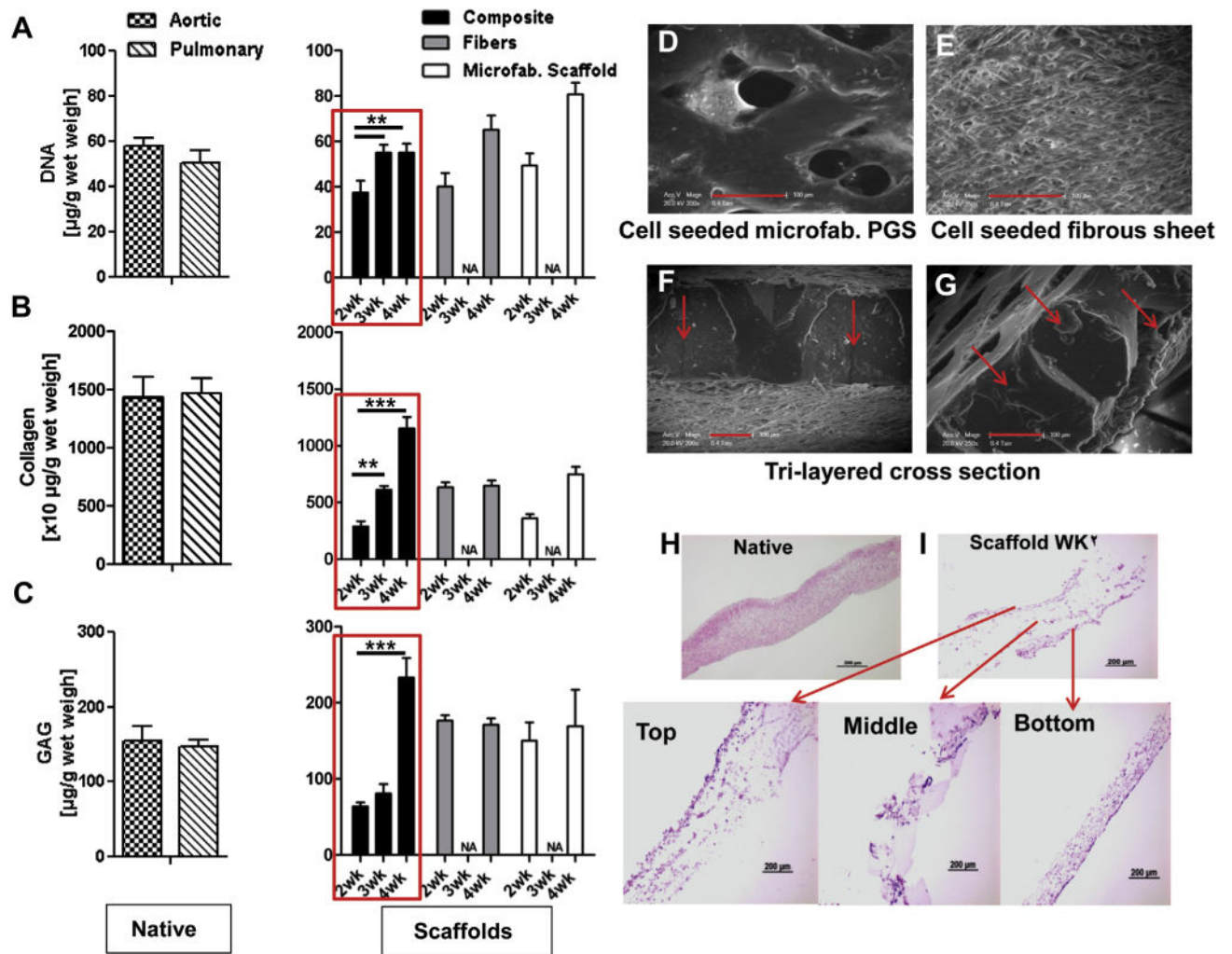


Fig. 7. *In vitro* assessment of tissue formation on engineered scaffolds. (A) DNA content, (B) collagen and (C) GAG production for AV and PV as well as cell-seeded scaffolds (fibrous, microfabricated PGS scaffold and tri-layered composites) cultivated for 4 weeks *in vitro*. DNA content increased with time for all three scaffolds. Collagen and GAG increased significantly with time for tri-layered scaffolds while the collagen and GAG concentrations were relatively constant for fibrous and microfabricated scaffolds. The ECM content and DNA concentration for cell-seeded tri-layered scaffolds were similar to native tissue, following 4 weeks of cultivation. (D) Cells and ECM were formed inside of the diamond pores of microfabricated scaffolds and (E) on the surface of fibrous scaffolds as observed in ESEM images. (F–G) ESEM micrographs from the cross-section of cell-seeded tri-layered scaffolds indicated the formation of a cell layer inside of the diamond pores (scale bars: 100 μm). (H) H&E staining of a native aortic leaflet and (I) a tri-layered scaffold following 4 weeks of cultivation, demonstrated the presence of cells and ECM in each layer of the scaffold, individual layers containing cells are shown as well (** $P < 0.01$ and *** $P < 0.001$).

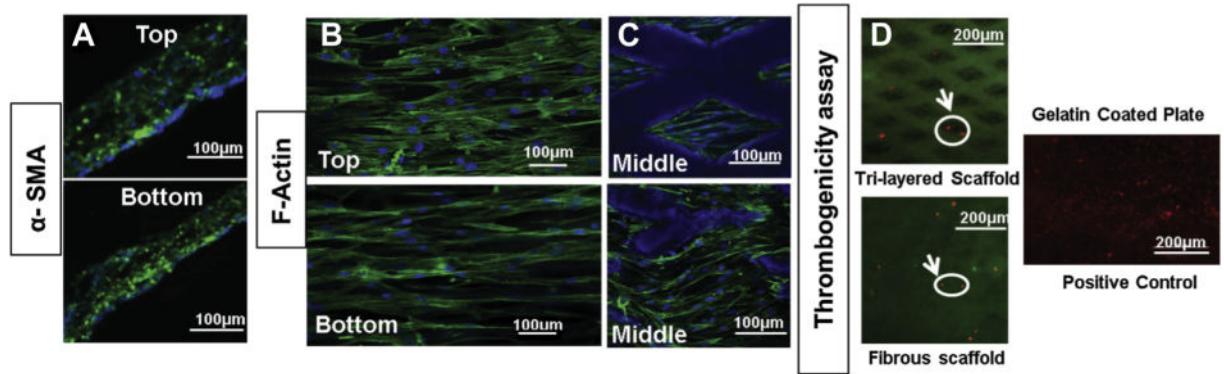


Fig. 8.

Immunostaining and thrombogenicity of cell-seeded tri-layered scaffolds. (A) α -SMA (green) and DAPI (blue) expression presented on both sides of tri-layered scaffolds. Representative images of MSCs immunostained for actin filaments (green) and nuclei (blue) on the (B) surfaces and (C) middle layers demonstrated that the scaffold structure guided the cell alignment toward the preferred direction in the fibrous and middle layers. (D) Thrombogenicity assay on the tri-layered composite scaffolds, demonstrating minimal platelet adhesion (red dots) on the surface of the scaffolds compared with number of platelets, attached to gelatin coated plates (positive control sample). (For interpretation of the references to color in this figure legend, the reader is referred to the web version of this article.)

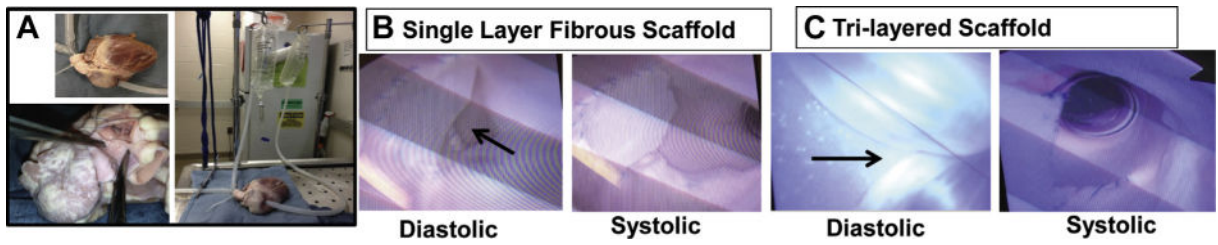


Fig. 9. Scaffold functionality as single leaflet replacement. (A) Experimental setup shows the hemodynamic functionality of the scaffolds as single leaflet substitutes in the PV position, assessed in an isolated heart model. (B) Endoscopic video images of the valve closing and opening demonstrated that fibrous scaffolds were insufficient in diastole. (C) Tri-layered scaffolds however, had adequate systolic performance and complete diastolic coaptation.

Table 1

Mechanical properties of tri-layered scaffolds at 0, 2wk and 4wk culturing time.

Tri-layered scaffolds	Tensile modulus (MPa)			$\bar{Y}\sigma$ (MPa)			$\bar{Y}\epsilon$		
	PD	XD	PD	PD	XD	PD	PD	XD	PD
Initial	3.02 ± 0.59	0.79 ± 0.09	0.59 ± 0.15	0.18 ± 0.03	0.60 ± 0.08	0.68 ± 0.18			
2wk	2.42 ± 0.54	0.57 ± 0.11	0.65 ± 0.06	0.21 ± 0.02	0.68 ± 0.19	0.67 ± 0.35			
4wk	2.83 ± 0.32	0.49 ± 0.15	0.63 ± 0.09	0.19 ± 0.05	0.58 ± 0.07	0.87 ± 0.27			